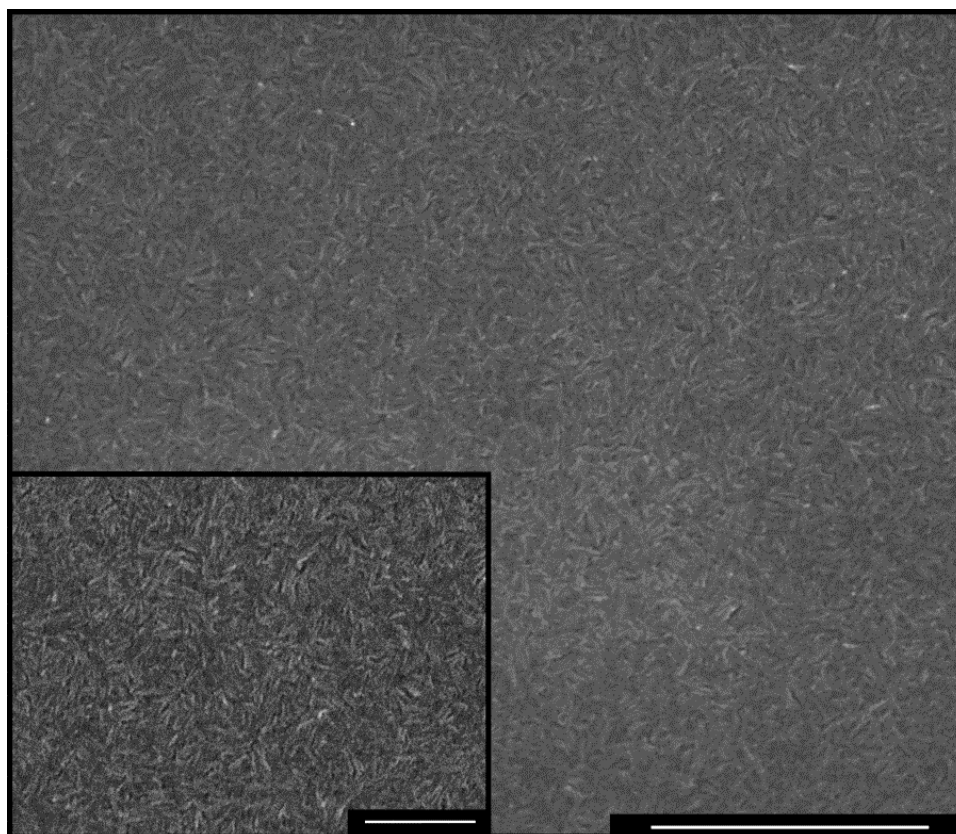


Supporting Information

Flexible all-inorganic nanocrystal solar cell by room-temperature processing

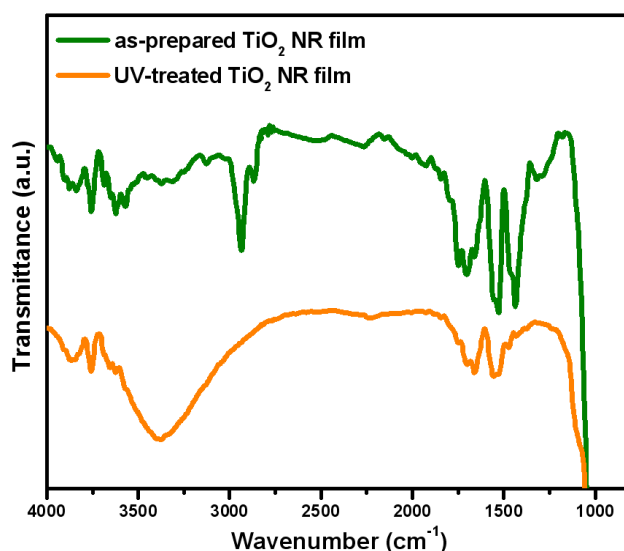
Anna Loiudice, Aurora Rizzo, Giulia Grancini, Mariano Biasiucci, Maria R. Belviso, Michela Corricelli, M. Lucia Curri, Marinella Striccoli, Angela Agostiano, P. Davide Cozzoli, Annamaria Petrozza, Guglielmo Lanzani, Giuseppe Gigli.

Figure S1. Top view Scanning Electron Microscopy (SEM) image of the TiO₂ NRs film (scale bar 500nm). In the inset a magnification of the image (scale bar 200nm). It is possible to observe that there TiO₂ layer is formed by disordered assembly of NRs. The irregular shape and surface defects of anatase TiO₂ NRs do not favour neither later nor vertical allignment upon the deposition onto a surface.



Supplementary Material (ESI) for Energy & Environmental Science
This journal is (c) The Royal Society of Chemistry 2011

Figure S2. FT-IR spectrum of as-synthesized TiO₂ NRs and of post-deposition UV-treated TiO₂ NRs on the silica substrate (the spectra have been normalied to the TiO₂ transmittance at 754 cm⁻¹). The IR spectrum of the untreated film displays characteristic narrow absorption bands at 2930 and 2850 cm⁻¹, which correspond to the antisymmetric and symmetric C–H stretching vibrations, respectively, of the –CH₂– moieties of the hydrocarbon chains.^{1,2} It can be noted that after UV irradiation the bands relative to the OLAC ligands are no longer observable, thus confirming that the removal of the carboxylic ligands from the TiO₂ surface has actually occurred. The broad absorption centred at ca. 3400 cm⁻¹ of the irradiated film can be ascribed to the stretching vibrations of O–H groups associated with water adsorbed both molecularly and dissociatively (terminal Ti–O–H moieties), which originates from UV-driven surface reaction and reconstruction processes in the presence of atmospheric water.



Supplementary Material (ESI) for Energy & Environmental Science
This journal is (c) The Royal Society of Chemistry 2011

Figure S3. FT-IR spectrum of as-synthesized PbS QDs and of post-deposition MPA-treated PbS QDs on the silica substrate (the spectra have been normalized to the PbS transmittance at 614 cm^{-1}). The IR spectrum of the untreated film displays the aliphatic groups in the region of the C-H stretch around 2900 cm^{-1} and the carboxylate stretching vibration around 1650 cm^{-1} . After the MPA treatment step, the aliphatic group band relative to the OLAC ligands are completely suppressed, that is indicative of highly efficient removal of oleic acid from the surfaces of the quantum dots. Most notably the carboxylate group band still appears, this is because MPA too contains a carboxylate group that is attached to the quantum dot surfaces.

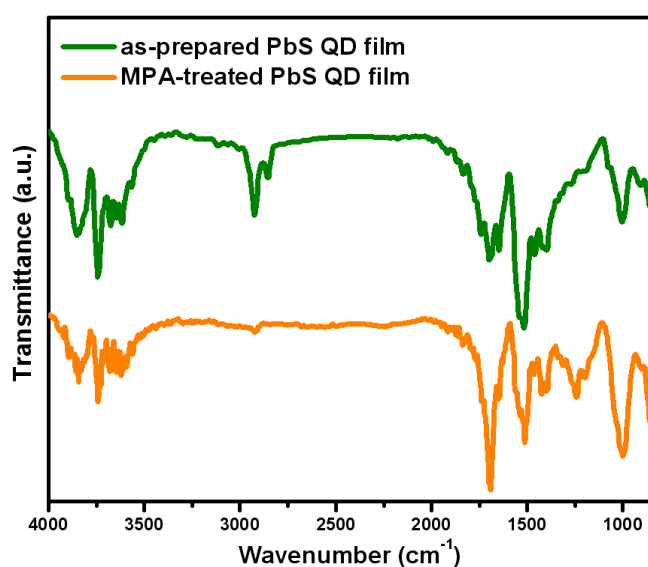


Figure S4.

Current density vs applied bias (J-V) characteristics under AM1.5 G (100 mWcm^{-2}) simulated solar illumination for the TiO_2 -NRs/PbS-QDs based solar cell with different active layer thicknesses. The best PCE is obtained for a device with TiO_2 /PbS thicknesses of 250nm/250nm.

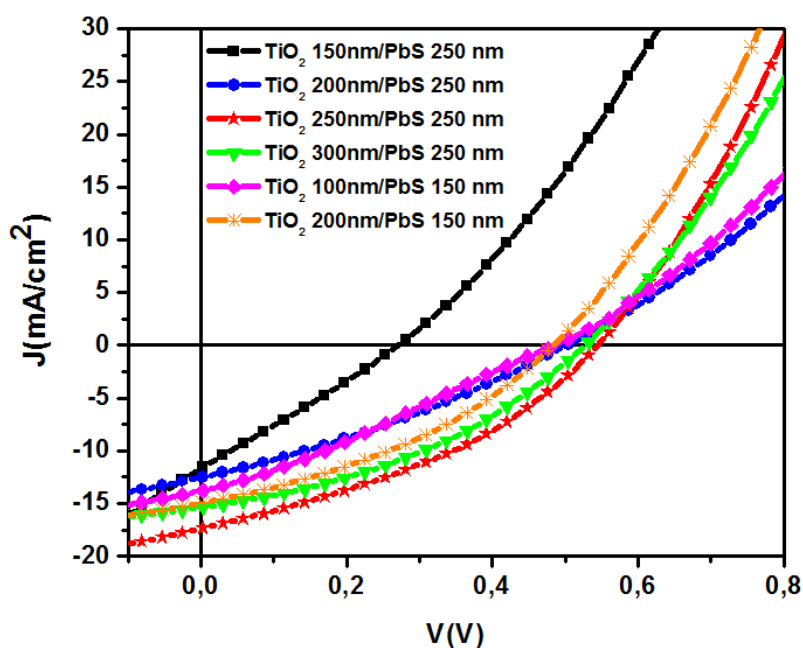


Table S1. Summary of Device Performance for different PbS/ TiO_2 active layer thicknesses.

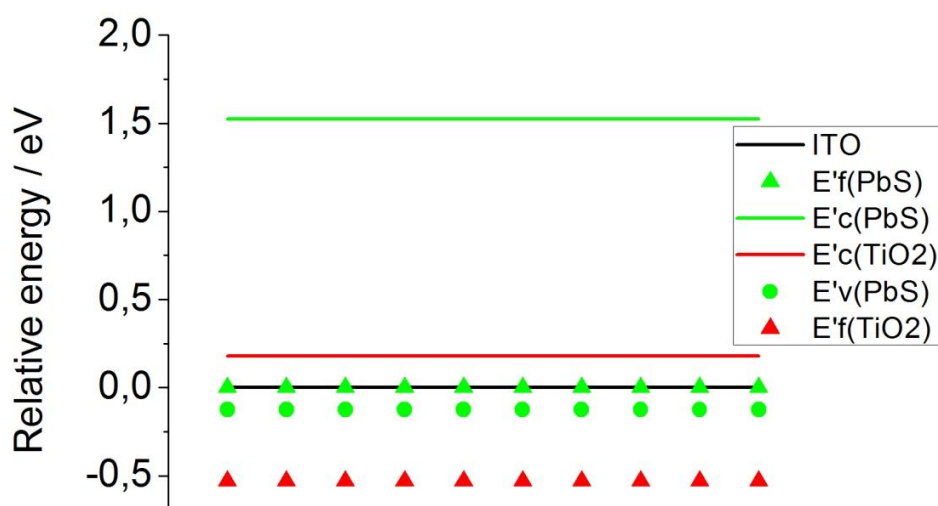
	PCE (%)	V_{oc} (V)	FF	J_{sc} (mA/cm^2)
TiO_2 (150nm)/PbS (250nm)	0,8	0,27	0,26	11,6
TiO_2 (200nm)/PbS (250nm)	2,2	0,51	0,34	12,5
TiO_2 (250nm)/PbS (250nm)	3,6	0,54	0,39	17,3
TiO_2 (300nm)/PbS (250nm)	3,0	0,53	0,37	15,4
TiO_2 (150nm)/PbS (150nm)	1,8	0,48	0,27	13,8
TiO_2 (200nm)/PbS (150nm)	2,6	0,49	0,37	14,3

The electron mobility of TiO_2 NRs film measured by means of electron-only device, i.e. by sandwiching the NR thin film between two Al electrodes, gives values of mobility in the order of $10^{-4} \text{ cm}^2 \text{ V}^{-1} \text{ s}^{-1}$.³ Considering that the electron mobility for TiO_2 NRs is similar to the

Supplementary Material (ESI) for Energy & Environmental Science
This journal is (c) The Royal Society of Chemistry 2011

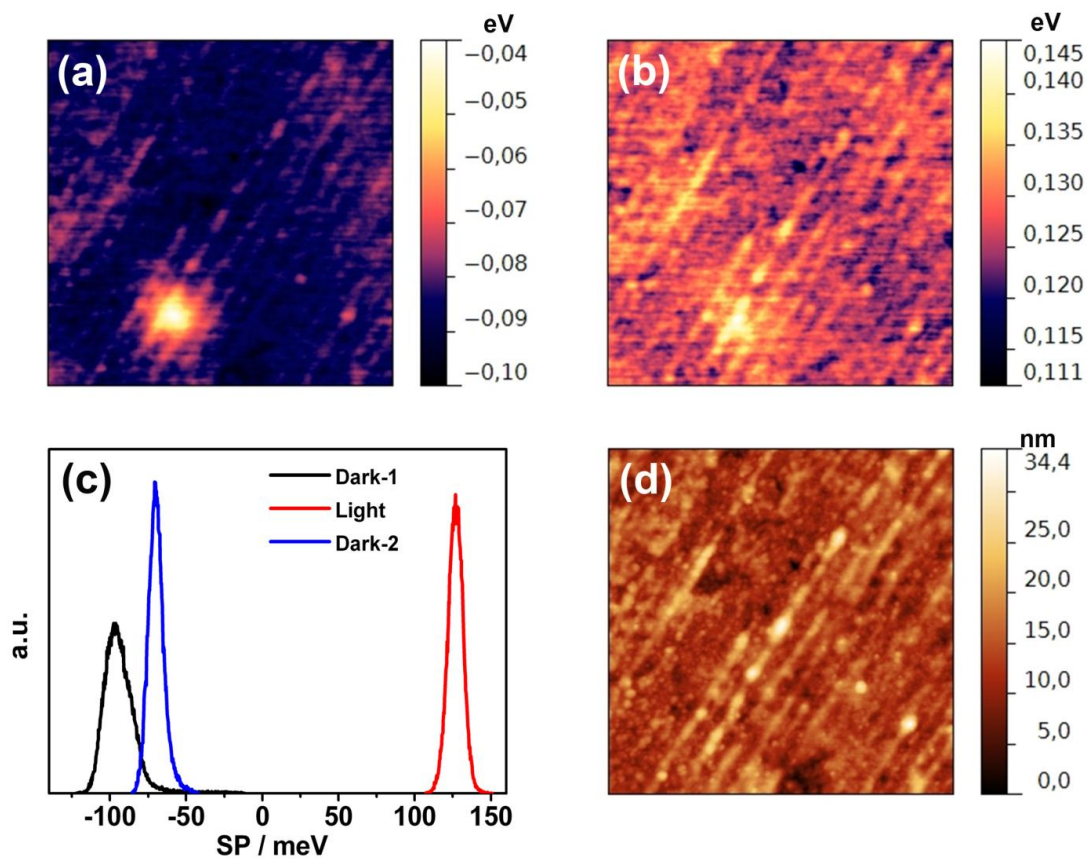
mesoporous TiO₂, we can assume an electron density of 10⁻⁶ cm⁻³ for the TiO₂ NRs as well. According to Sargent et al.^{4,5} the depletion region in PbS/TiO₂ device is around 200nm and is distributed between the two semiconductors. The thickness of our best device is larger than the depletion width, indeed in order to obtain a good light absorption in the bilayer device geometry the thickness of the PbS should be increased up to 250 nm, which will lead to considerable carrier recombination losses. From our experiments we can conclude that the 250 nm/250 nm is the best compromise between light absorption and charge recombination losses in the net bi-layer heterostructure.

Figure S5. Band positions relative to a Pt/Ir conductive tip for PbS, TiO₂ layers and work function of ITO. The valence and conduction bands for the PbS are carried out from the Fermi level measurement performed by KPFM. The fermi level of the TiO₂ is measured by KPFM. The conduction band value of TiO₂ was taken from literature.^{5,6}



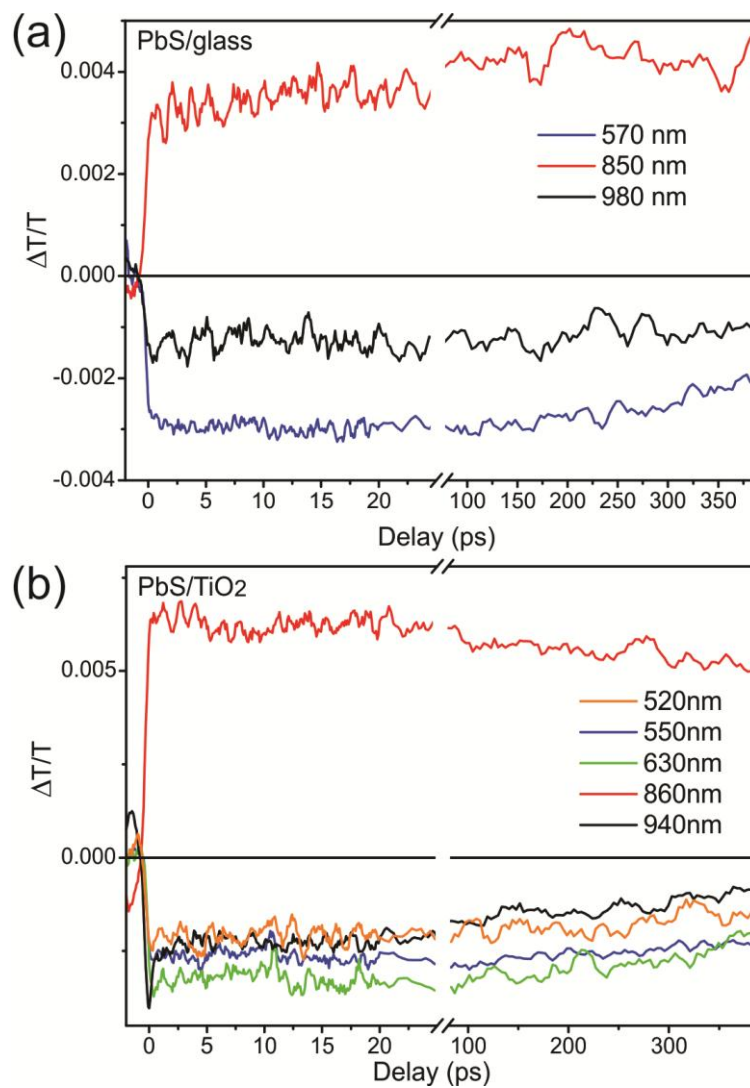
Supplementary Material (ESI) for Energy & Environmental Science
This journal is (c) The Royal Society of Chemistry 2011

Figure S6. Surface potential images under (a) dark and (b) illumination. (c) Histogram distribution of the surface potential under three different conditions: before illumination (labeled “dark-1”), under illumination (labeled “light”), and after illumination (labeled “dark-2”). (d) AFM image of ITO/PbS device. The scan size of images is $2\ \mu\text{m} \times 2\ \mu\text{m}$.



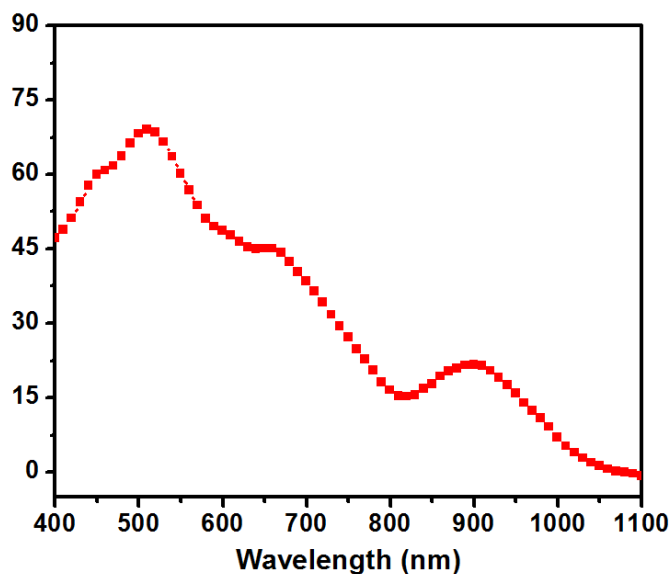
Supplementary Material (ESI) for Energy & Environmental Science
This journal is (c) The Royal Society of Chemistry 2011

Figure S7. $\Delta T/T(\tau)$ dynamics in the first 400 ps time window at selected probe wavelengths (see the legend) of (a) PbS QDs on glass substrate and of (b) PbS-QDs/TiO₂-NR.



Supplementary Material (ESI) for Energy & Environmental Science
This journal is (c) The Royal Society of Chemistry 2011

Figure S8. IPCE spectrum for the PbS-QDs/TiO₂-NR solar cell on PET substrate.



¹ Caputo, G.; Nobile, C.; Kipp, T.; Blasi, L.; Grillo, V.; Carlino, E.; Manna, L.; Cingolani, R.; Cozzoli, P. D.; Athanassiou, A. *J. Phys. Chem. C* **2008**, 112, 701–714;

² Silverstein, R. M.; Webster, F. X. *In Spectrometric Identification of Organic Compounds*, John Wiley & Sons, Inc., 6th edn, **1997**.

³ Liao H.-C., Lee C.-H., Ho Y.-C., Jao M.-H., Tsai C.-M., Chuang C.-M., Shyue J.-J., Chen Y.-F., Su W.-F. *J. Mater. Chem.* **2012**, 22, 10589–10596.

⁴ Barkhouse D. A. R., Debnath R., Kramer I. J., Zhitomirsky D., Pattantyus-Abraham A. G., Levina L., Etgar L., Grätzel M., Sargent E. H. *Adv. Mater.* **2012**, 24, 2315–2319.

⁵ Pattantyus-Abraham A. G., Kramer I. J., Barkhouse A. R., Wang X., Konstantatos G., Debnath R., Levina L., Raabe I., Nazeeruddin M. K., Grätzel M., Sargent E. H. *ACS nano* **2010**, 4, 3374–3380.

⁶ Wang, J.; Zhang, T.; Wang, D.; Pan, R.; Wang, Q.; Xia, H. *Chem. Phys. Lett.* **2012**, 541, 105–109.

⁷ Grätzel, M. *Nature* **2001**, 414, 338–344.